Compatibilization of an immiscible blend of EPDM and POM with an Ionomer

Mario Bragaglia[1], Tony McNally[2], Francesca R. Lamastra[1], Valeria Cherubini[1], Francesca Nanni[1*]

(1) University of Rome "Tor Vergata", Department of Enterprise Engineering "Mario Lucertini", and INSTM RU Roma-Tor Vergata, via del Politecnico 1, 00133 Rome, Italy

(2) International Institute for Nanocomposites Manufacturing (IINM), WMG, University of Warwick, CV4 7AL, UK

*Corresponding author: E-mail: fnanni@ing.uniroma2.it (Francesca Nanni)

Abstract

Immiscible blends of ethylene-propylene-diene-monomer (EPDM) and polyoxymethylene (POM), when EPDM is the major phase were compatibilized on the addition of an ionomer, poly(ethylene-co-methacrylic acid). The inclusion of the ionomer reduced the interfacial tension between the two phases, such that the diameter of the POM domains were significantly reduced to between 0.5μm and 2μm, typical of that required to toughen ductile polymers. The mechanical properties of the resultant compatibilized blends were significantly enhanced with increases in Young's modulus (↑54%), tensile strength (σ, ↑139%), elongation at break (ε, ↑97%) and tensile toughness (↑500%) with increasing ionomer content, relative to EPDM rubber alone. The ShoreA hardness of the compatibilized blend was 70.1 compared to 56.8 for the immiscible binary blend and, 50.2 for neat EPDM rubber.

1. Introduction

One of the most promising routes in the development of new materials continues to be via the production of polymer blends. Polymer blending provides a route, (i) to achieving a material having a combination of the unique properties of each component; (ii) a reduction in material cost with little or no loss of properties and (iii) for the improvement of material processability [1]. Polymer blends constitute almost a third of the global plastic market [2] since they allow a rapid development of modified polymeric materials to meet emerging needs bypassing the need for polymerization. When two polymers are mixed together, they can form a miscible, partially miscible or an immiscible blend.

The former is a new single-phase material showing averaged properties of the two components, the latter is a material with two separate phases having a weak interface [3], where the lack of interaction between the two components results in poor mechanical properties. Miscibility is the ability of a mixture to form a single phase over a certain temperature range, pressure and composition. It is the result of interactions between the blend components, such as hydrogen bonding, dipole-dipole, van der Waals (as dispersion forces) and trans-reactions [4]. The possible material combinations for blending are theoretically endless, but certain thermodynamic conditions must be respected for complete miscibility of a polymer blend [5]. The Gibbs free energy for mixing, ΔG_{mix} (Eq.1) and the enthalpy of mixing, ΔH_{mix} (Eq.2) must be negative, while the second derivative of Gibbs free energy of mixing (Eq.3), with respect to volume fraction (ϕ), must be positive.

$$\Delta G_{mix} < 0 \; or \; \Delta G_{AB} < \Delta G_A + \Delta G_B \qquad (1)$$

$$\Delta H_{mix} - T\Delta S_{mix} < 0 \qquad (2)$$

$$\left(\frac{\partial^2 \Delta G_{mix}}{\partial \phi^2}\right)_{T,p} > 0 \qquad (3)$$

Blends of two or more thermoplastics or elastomers, or a combination of these, are appealing given the possible combinations [6]. In particular, thermoplastic-rubber blends are very promising materials since they combine the unique properties of vulcanized rubbers (i.e. high elongation at break and elastic recovery) with the higher mechanical properties of easily processable thermoplastics (elastic modulus and mechanical strength) [7–11]. Thermoplastic-rubber blends are usually classified in to two categories, depending on which properties of the blend components to be modified. By way of example, (i) a rubbery phase added to a brittle polymer to increase toughness and elongation at break or (ii) a rigid phase added to a rubber to increase strength and decrease its tendency to flow or to undergo permanent deformation when under load [12–15].

Polyoxymethylene (POM) and ethylene-propylene-diene-monomer (EPDM) are an interesting combination as both are individually used in several applications across a number of sectors, from automotive to home appliances [16]. EPDM is elastic and has good aging resistance [17–19] and POM has high hardness, good fatigue life under cyclic loadings, a low coefficient of friction (with inherent lubricity), good resilience, tensile strength and stiffness over a wide temperature range [20,21]. POM/EPDM blends, where POM is the major phase, are immiscible, having well separated domains with strong interfacial tension. Moreover, an increase in the EPDM content results in a decrease in tensile strength and elastic modulus, while impact strength and elongation at break reaches a maximum at low EPDM content, i.e. ≤10% by weight, before drastically decreasing due to incompatibility between phases [22]. Other studies have shown that the addition of EPDM did not alter the crystalline structure of POM, but slightly decreased the crystalline content and the apparent crystallite size (ACS), calculated using the Scherrer equation [23]. Moreover, the EPDM vulcanization process when using dicumyl peroxide (DCP), reduced the interfacial tension between the POM and EPDM phases resulting in a slight shift of the glass transition temperatures of both components, although the blend remained immiscible [24].

To alter the immiscibility of a polymer blend, compatibilization is required, i.e. the addition of a third component that reduces the interfacial tension between phases. Compatibilizers are generally molecules with both hydrophobic and hydrophilic properties that can locate to the interfaces between the two polymer phases. A reduction in interfacial tension facilitates better mixing of the blend components, stabilizes the blend morphology during processing and promotes adhesion between phases, resulting in improved mechanical properties of the blend [25]. However, compatibilization can also have some negative effects, e.g. it can reduce thermal stability and the degradation temperature of the blend [26] .

Several compatibilization strategies have been developed [2,6,27] including, addition of (i) a small quantity of co-solvent, a third component, miscible with both phases, (ii) a copolymer partly miscible with both phases [28], (iii) a large amount of a core-shell copolymer, (iv) a small quantity of

nanoparticles which influence the blend structure similar to particle-stabilized water/oil emulsions [4] and (v) reactive compounding that leads to the modification of at least one macromolecular species and results in the development of regions of local miscibility [29].

There have been some attempts to improve the properties of blends of POM/EPDM using different compatibilizers, such as poly(acrylic-acid)-grafted-polypropylene (PGP) [24], maleated EPDM (MEPDM) [30], ethylene-vinyl acetate (EVA) [22] and maleic anhydride grafted EPDM (EPDM-g-MAH) [26], each had a different effect on tensile and impact strength. Inclusion of (≤ 8 wt%) PGP and EPDM-g-MAH (≤1 wt%) resulted in both the tensile and impact strength increasing with increasing compatibilizer content. Addition of MEPDM and EVA also yielded increased tensile and impact strength, but only for low compatibilizer content (≤5wt%) as both properties drastically decreased with further additions due to coalescence of the elastomeric phase. Ionomers have also been used as compatibilizers [31]. Ionomers are olefin-based polymers containing a small percentage of ionic groups characterized by strong ionic inter-chain forces that have a primary role in controlling properties [32]. They can also be defined as polymers in which the bulk properties are determined by ionic interactions in discrete regions of the material also called ionic aggregates [33,34]. Ionomers are copolymers composed of non-ionic and ionic repeating units and, because of the opposite polarity the non-polar chains are grouped together, while the polar ionic groups are attracted together. The ionic groups can be either located randomly or systematically within the primary polymer chain, as end groups on polymer chains, or as segment in a block copolymer [35]. Ionomers can interact in different ways with other polymers, via ion-ion, ion pair-ion pair, ion-coordination and ion-dipole interactions [36,37]. As a compatibilizer, ionomers can be used as ion-dipole interactions enhance miscibility in polymer blends [38–42]. It is known that polar polymers can interact strongly with some small ions, so if ionic groups are introduced into a polymer, thus creating an ionomer, strong interactions could result with polar polymers via ion-dipole interactions. Despite the sustained growth in research outputs and patents on ionomers, the number of commercially available ionomers remains relatively small. Some common ionomers include (poly(ethylene-co-methacrylic acid)) ionomers (e.g.

Surlyn®) and perfluorosulfonate ionomers (e.g. Nafion®), both manufactured by DuPont. Moreover, the addition of ionomers to thermoplastic-elastomer blends can confer self-healing properties as reported previously [43].

In this work, we investigate the compatibilization of a blend of EPDM and POM with POM as the dispersed phase, with the goal of increasing the stiffness and strength of the rubber component. To date, the published literature on this topic has been limited and the articles on POM/EPDM blends has focused on POM as the major phase, in order to increase the toughness of the POM matrix with EPDM rubber as the dispersed phase [12,22,24,26,30,44]. In this study, POM was added, as a reinforcement phase to an EPDM matrix with a view to increasing mechanical properties, such as the tensile strength of the rubber. Poly(ethylene-co-methacrylic acid)-Zn^{2+} ionomer (EMAA-Zn^{2+}) was chosen as a compatibilizer due to its non-polar component having similar chemistry to EPDM and its polar component capable of dipole interactions with POM. The EPDM/POM and EPDM/POM/EMAA blends were prepared in a batch mixer and then vulcanized. The resultant blend morphology was characterised and correlated with the mechanical and thermal properties obtained using a range of techniques.

Experimental

EPDM (Dutral® 4047) was purchased from ENI-Versalis. POM (Delrin® 500) was supplied by DuPont. Dicumyl Peroxide (DCP) was purchased from Sigma-Aldrich, the purity (TLC) of the material was 98%. Surlyn® 9020, an ionomer of ethylene and methacrylic acid (EMAA) neutralised with 73% Zinc oxide (ZnO), was provided by DuPont (EMAA-Zn^{2+}).

All blends were prepared by melt mixing using an HAAKE Rheomix OS Lab Mixer, at 190 °C and 40 rpm. Firstly, EPDM was masticated in the mixer chamber for 5 minutes, second, POM was added to the chamber and both materials mixed for 7 minutes. Lastly, for EPDM/POM uncompatibilized blends, DCP was added into the chamber, whereas, for EPDM/POM/EMAA-Zn^{2+} 'compatibilized' blends, the ionomer was added followed by the DCP after 2 minutes. In both cases dynamic vulcanisation took 5 minutes after the peroxide addition. For all blends, the EPDM:POM

composition was fixed as 80:20 (wt%) and the DCP content was fixed at 4 phr (parts per hundred of rubber). Compatibilized blends were prepared with increasing ionomer loading, 5 wt%, 10 wt% and 20 wt%, relative to the total weight of EPDM and POM. The sample code names and blend composition are listed in **Error! Reference source not found.**.

Table 1. Composition of EPDM/POM/EMAA blends

Sample Code	EPDM (wt%)	POM (wt%)	EMAA-Zn^{2+} (wt%)	DCP
EPDM:POM	80	20	0	4 phr
EPDM:POM -5	80	20	5	4 phr
EPDM:POM -10	80	20	10	4 phr
EPDM:POM -20	80	20	20	4 phr

During the mixing process the rheological behaviour of blend was evaluated from the torque versus time curves. For each composition, plaques of both uncured (i.e. from the melt mixing process) and cured samples (i.e. samples hot pressed into sheets using a Dr. Collin P200P platen press machine) were prepared. During curing, the compounds were subjected to a pressure of 200 bar and a temperature of 160 °C for 17 minutes, followed by 5 minutes at 50 °C maintaining the applied pressure. A degassing process was performed after hot pressing.

X-Ray Diffraction (XRD) measurements were performed using Philips X'Pert Pro diffractometer equipped with a Cu target. The scans were carried out with a step size of 0.02°/step and a time step of 2 s/step over a 2θ range of 10-80°.

FTIR Spectroscopy was performed using a Jasco FT/IR-6600 spectrometer, equipped with ATR PRO ONE Single-reflection ATR (attenuated total reflectance) accessory. The spectra were collected in the spectral range 4000-600 cm^{-1}, with 4 cm^{-1} resolution and each spectrum averaged over 32 scans.

DSC measurements were carried out using a Mettler-Toledo TGA-DSC1 STARe instrument, under flowing nitrogen. Samples (10 mg) were sealed in aluminium pans and heated from room temperature (RT) to 250 °C (300 °C for "cured" samples) at a heating rate of 10 K/min, then the

154 samples were held at 250 °C (or 300 °C) for 1 minute and cooled to -80 °C at 10 K/min using liquid
155 nitrogen as coolant. All samples were then reheated again to 250 °C (300 °C for "cured" samples) at
156 10 K/min, held at 250 °C (or 300 °C) for 1 minute and cooled to RT at 10 K/min. Melting temperature
157 (T_m) and crystallinity degree (X_c,%) were evaluated using the Mettler-Toledo STARe evaluation
158 software. The following equation was used to calculate the degree of crystallinity from DSC analysis:

159 $$X_c = \frac{\Delta H_m}{\Delta H_f(1-m)} \quad (4)$$

160 where, $\Delta H_m$is the enthalpy of fusion on melting, measured by the area under the endothermic peak
161 and ΔH_f is the enthalpy of fusion of a theoretically 100% crystalline POM [45] and (1-m) is the nominal
162 weight fraction of POM.

163 TGA was carried out using a Mettler-Toledo TGA-DSC1 STARe instrument, under flowing
164 nitrogen. Tests were performed heating the samples from room temperature up to 500 °C at the
165 heating rate of 10 °K/min.

166 The viscoelastic properties of all blends were investigated in tensile mode using a Triton 2000
167 DMTA instrument Triton Technology, in the temperature range −100 °C to 200 °C using a heating
168 rate of 3 K/min applying a displacement of 0.05 mm at a frequency of 1 Hz. The glass transition
169 temperature (T_g) was evaluated as the temperature corresponding to the peak maximum in the loss
170 tangent (tanδ) curve.

171 Tensile testing of blends was carried out according to ASTM D638, standard for plastic
172 materials. The samples with a geometry in accordance to ASTM D638 "type V" were cut out from
173 the pressed sheets, therefore only the cross-linked "cured" samples were mechanically tested. Tests
174 were performed using a Lloyd LRX tensile testing machine, equipped with 50 N load cell and setting
175 the crosshead speed to 500 mm/min.

176 The Shore A hardness of the samples was carried out in accordance with ASTM D2240 using
177 a Shore A digital durometer manufactured by Fervi. Measurements were taken at regular intervals at

least 12 mm from the edge and 10 mm apart. A minimum of five readings were taken for each specimen.

The morphology of the blends was imaged using a Field Emission SEM (FEG-SEM) LEO SUPRA 35 Zeiss instrument working with accelerating voltage of 5 kV. Prior to imaging, cryo-fractured specimens were immersed in acetic acid or sodium hydroxide (NaOH) solution for 24 h for preferential etching of the POM phase. The non-conductive etched samples were then sputter coated with a layer of gold with an approximate thickness of 10 nm. Analysis of the images obtained for the dispersed phase was carried out using ImageJ software.

2. Results and Discussion

In the first instance, the thermal properties of the individual components were recorded. Figure 1 a) shows the DSC scan for neat EPDM in the region −70°C - 0 °C. The glass transition temperature (T_g) can be detected at −52 °C, and the melting temperature (T_m) of a very small crystalline fraction at −25 °C [4647]. The melting peak is very small because it is derived from the melting of a few ethylene sequences of EPDM, estimated at being less than 1% crystalline [48,49]. The DSC heating and cooling scans for POM are shown in Figure 1 b) and c). The polymer displays two different melting temperatures (T_m) during the first and second heating at 182 °C and 173 °C (Figure 1b)), whereas the peak crystallisation temperature (T_c) is at 148 °C in both cooling cycles (Figure 1c)) [50]. This behaviour shown by neat POM can be explained by considering that POM exhibits different crystal morphologies, i.e. the folded-chain crystal (FCC) and extended-chain crystal (ECC). Each morphology shows a different time dependent melting behaviour and different T_m, for instance, the equilibrium melting point of extended POM chain crystals from literature is 182.5°C [51]. So it is likely that the POM used in this study had initially an ECC morphology that changed to a mixed FCC and ECC morphology after the first DSC cooling cycle.

The degree of crystallinity X_c was evaluated according to [21] considering the enthalpy of fusion, ΔH_m of a theoretically 100% crystalline POM was taken as 326 J/g. X_c was found to be 46% and 53% respectively, from the first and second heating cycles.

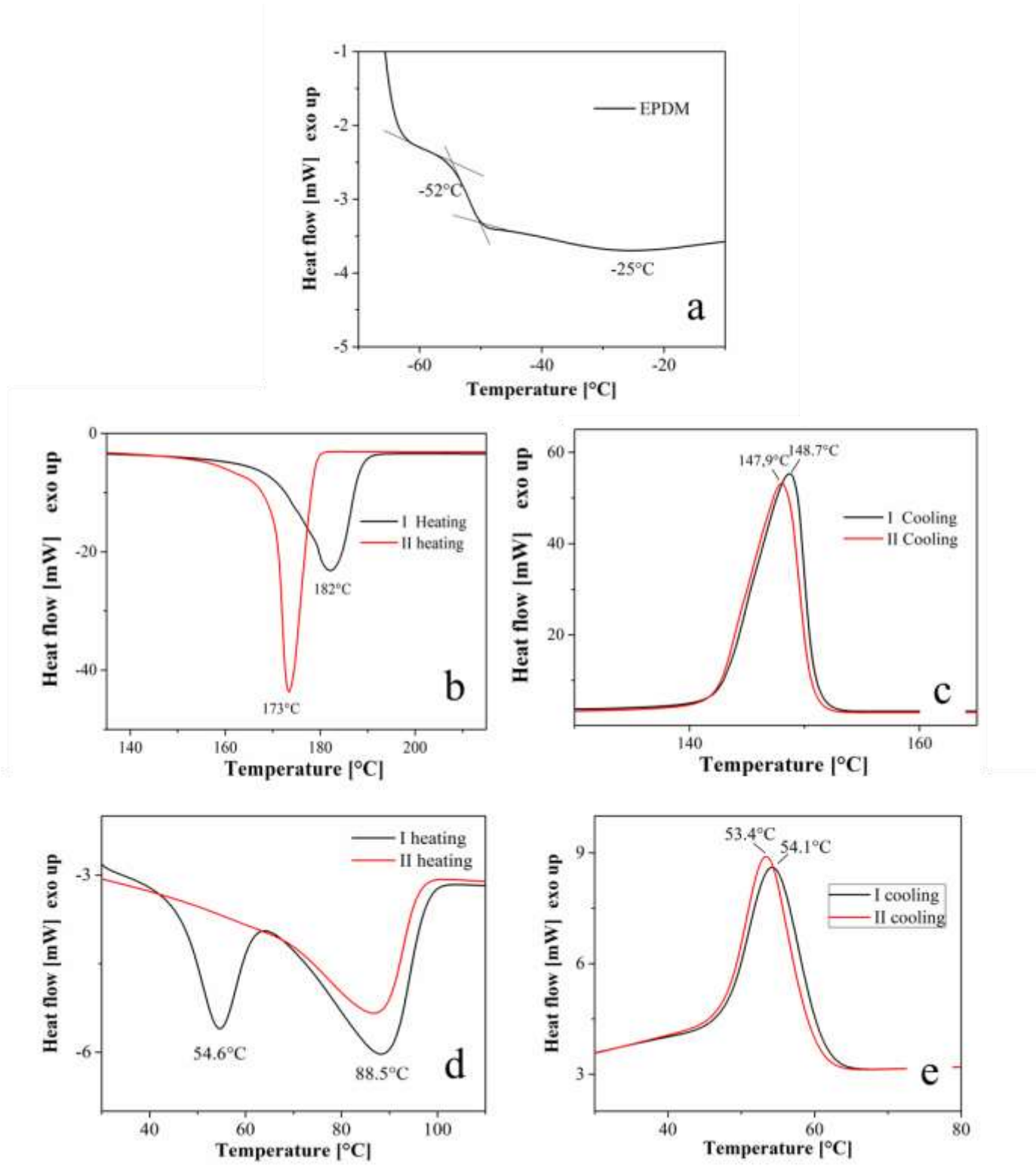

204

205 **Figure 1.** DSC traces showing the T_g of EPDM (a), melting peak (b) and crystallization peak (c) for

206 neat POM and, melting peak (d) and crystallization peak (e) for neat EMAA-Zn^{2+} ionomer.

The DSC thermogram of the neat EMAA-Zn^{2+} ionomer shows two endothermic peaks in the first heating scan (Figure 1d) and e)). The peak at higher temperature is associated with the T_m of polyethylene crystals at 88 °C, while the lower temperature peak at 54 °C is derived from the melting of small PE secondary crystals that slowly form after the primary crystallisation process [52–54]. However, other studies, first proposed by Tadano *et al.* [55], attribute this lower temperature peak to an order-disorder transition (T_i) within the ionic aggregates [56,57]. In agreement with this work, only the polyethylene melting process is observed (at 88 °C) n the second heating cycle, while no second endothermal peak is recorded. In both the first and second cooling cycle, only the crystallisation peak of the polyethylene component at 54 °C is recorded. Figure 2 shows the DSC scans for the uncured binary EPDM:POM blend. The first heating scan (Figure 2 a)) shows a T_m at 168 °C associated with the POM dispersed phase [58]. A second endothermic process occurring at 226 °C is derived from the degradation of the POM phase, most likely from low molecular weight chains [59]. To confirm this hypothesis, TGA was carried out on both cured and uncured EPDM:POM samples (Figure 2 c) and d)), where there is some evidence for the decomposition of the POM phase starting just above 200°C, in agreement with the DSC results [60]. Therefore, it can be expected that blending and/or the curing process may affect the thermal stability of these blends [27].

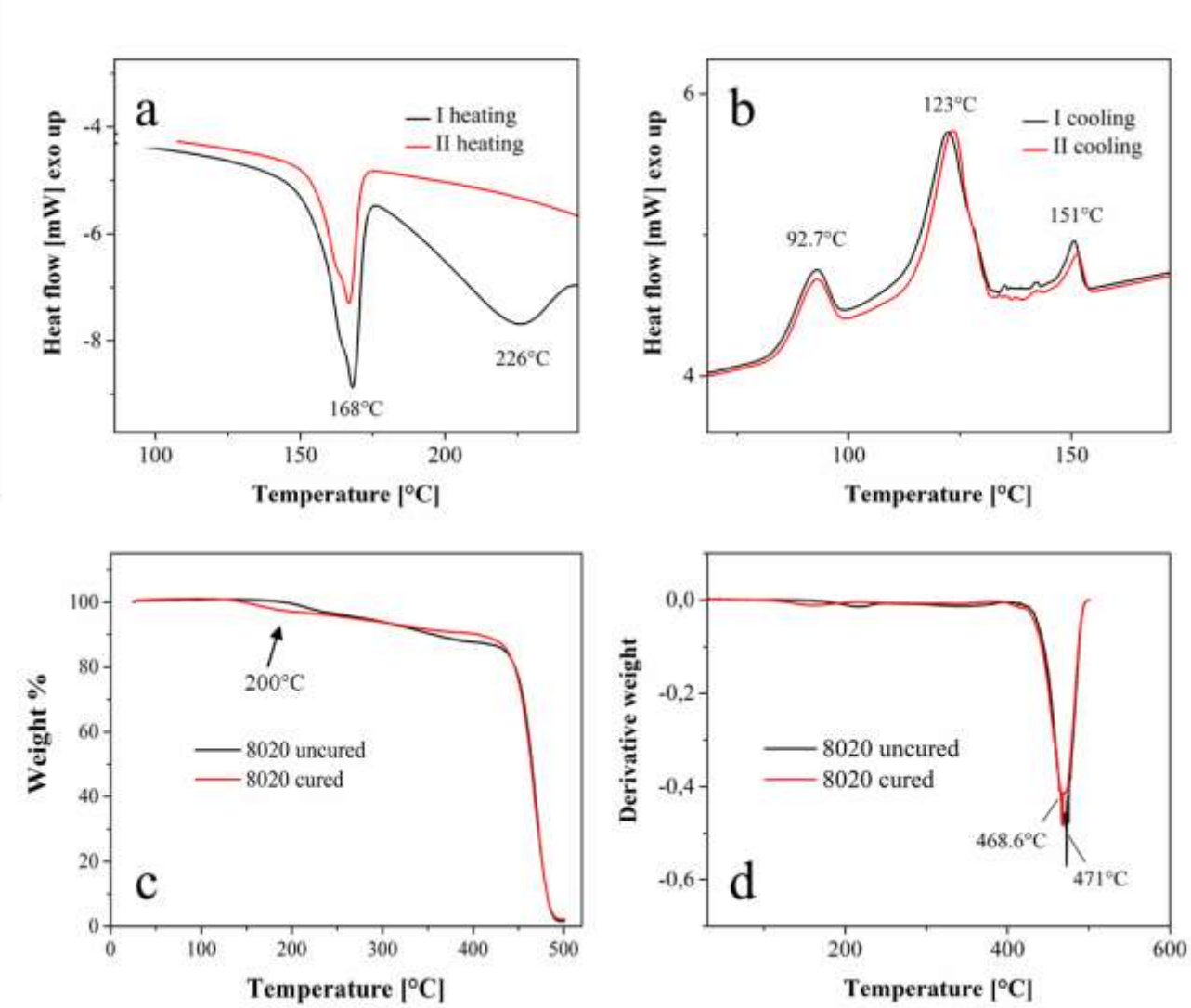

Figure 2. DSC melting (a) and crystallization (b) of the EPDM-POM blend and, (c) TGA weight loss curve for the EPDM-POM blend and (d) corresponding derivative plot.

The cooling scans of the uncured 80:20 sample (Figure 2 b)) displays three crystallisation peaks at 93 °C, 123 °C and 151 °C which are associated with the so-called fractionated crystallisation phenomenon, a peculiarity of blends with a crystallisable dispersed phase in an amorphous matrix. This behaviour arises from subsequent steps of primary nucleation occurring at different stages of undercooling, ΔT_c, sometimes resulting in a single crystallisation peak at the homogeneous nucleation temperature ($T_{c,hom}$) [61,62]. Koutsky *et al.* [63] demonstrated that fractionated crystallisation is directly

related to the size of the areas of the dispersed insoluble phase, also called droplets, in the matrix. Frensch *et al.* proposed a mechanism for this phenomenon [64]. Heterogeneities are fundamental for nucleation and crystallisation processes, and when a crystallisable polymer is dispersed into small droplets, the heterogeneities are also distributed in the dispersed polymer phase. Depending on the size and the number of the dispersed domains, they can contain one or more heterogeneities available for nucleation and primary crystallization [65]. If the size of the droplets of the dispersed polymeric phase is very small, it may happen that not every droplet contains one heterogeneity of "type 1" (i.e. the type of heterogeneity which requires the lowest degree of undercooling ΔT_c). As a consequence, only a limited part of the dispersed phase, i.e. those droplets containing the type 1 heterogeneity, will be able to crystallise at an undercooling ΔT_{c1}, through primary crystallisation. Moreover, since the droplets are not in contact with each other, further growth via secondary nucleation in other crystallisable droplets is impossible. During further cooling, heterogeneities of "type 2" requiring the second lowest degree of undercooling, ΔT_{c2}, can become active in some of the remaining droplets, resulting in a second crystallisation exothermic peak (i.e.at 123°C in Figure 2b)). This process continues until eventually some very fine droplets that have not yet been nucleated by the heterogeneous species, crystallise in a homogeneous mode [62,66]. The range of undercooling at which several crystallisation steps occur, depends on the type of heterogeneities available in the melt [65]. Fractionated crystallisation was first reported for POM for PE/POM blends and then with other polymers [62,67–70]. Fractionated crystallisation is often accompanied by a large decrease in the degree of crystallinity (X_c) of the dispersed phase [71] compared to the bulk material, and this decrease can also be observed in the present study. The crystalline content of the POM when the dispersed phase was 32% from the first heating cycle and 21% from the second, while it was 46% and 53% from the first and second heating cycles for the POM homopolymer.

The addition of the ionomer alters the thermal transitions of the uncross-linked blends. Beside the presence of the endothermic peaks related to the melting of the ionomer, as shown in figure 3 a), it is evident there is a shift of the T_m of POM, from 168°C to 171°C with increasing ionomer content,

especially during the second heating cycle. That this melting transition shifts with the addition of ionomer suggests that there is an interaction between the blend components altering the microstructure of the system [72]. Again, the presence of the ionomer has a visible impact on the cooling scans of the uncross-linked blends (Figure 3 b)) as the temperatures of the crystallisation peaks, derived from the POM phase, decrease towards lower values. In fact, the POM crystallization peak having T_c at 150°C in the uncross-linked blend without ionomer, tends to disappear in these samples with increasing ionomer loading, (i.e. sample 80:20-20) and the resulting crystallization peak for POM phase occurs at 97°C.

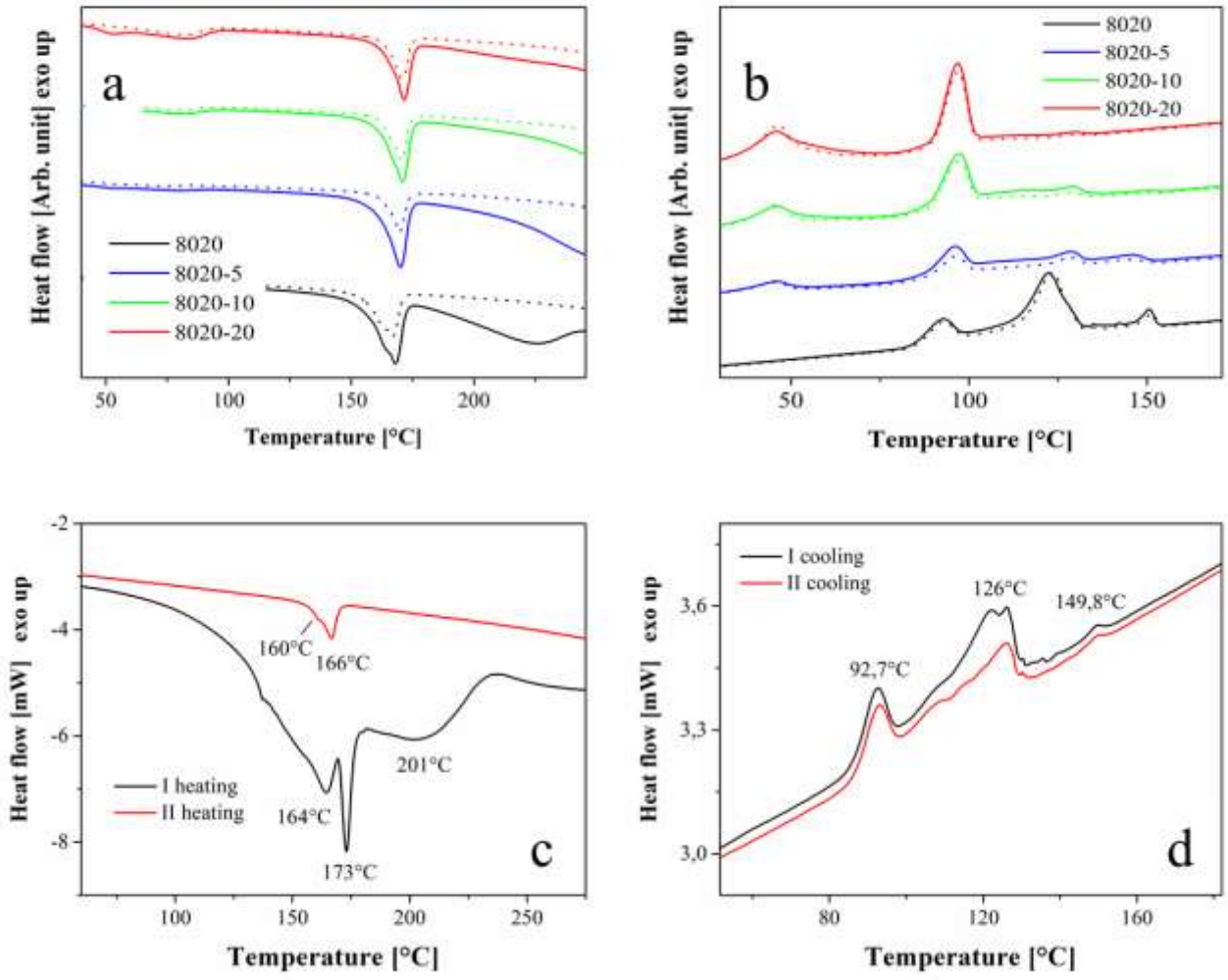

Figure 3. DSC a) heating and b) curves for uncross-linked blends of EPDM:POM; Zn^{2+}Ionomer and, c) heating and d) cooling curves for (80:20) EPDM:POM cross-linked blend.

This observation may be a result of increased compatibilization when the size of the droplets of the dispersed phase is reduced, leading to a shift in crystallization to lower temperatures and finally resulting in a homogeneous crystallization process [66,73]. The degree of crystallinity (X_c) slightly decreases with increasing ionomer content, from the first heating cycle, while in the second there is no progressive decrease with ionomer content, although X_c is lower than for the samples without ionomer, as summarised in Table 2.

Table 2. Thermal parameters determined from DSC measurements for un-crosslinked EPDM:POM and EPDM:POM\: Zn^{2+} Ionomer blends.

Parameter	EPDM:POM	EPDM:POM-5	EPDM:POM -10	EPDM:POM -20
T_i	-	53	53	53
$T_{m,ion,1H}$	-	81	81	83
$T_{m,ion,2H}$	-	74	80	81
$T_{m,\ POM\ 1H}$	168	170	170	171
$T_{m\ POM,2H}$	167	170	171	171
$T_c$ion	-	46	46	46
$T_{c1,2,3}$ POM	93-122-160	96-129-146	97-129	97-129
$\Delta H_{m,1H}$ [J/g]	20.6	18.8	16.8	13.4
$X_{c,1H}$ [%]	32	30	28	25
$\Delta H_{m,2H}$ [J/g]	13.5	8.3	10.5	9
$X_{c,2H}$ [%]	21	13	16	14

The first heating scan of the cross-linked EPDM:POM sample shows two melting temperatures, at 164 °C and 173°C, related to the melting of the ECC and FCC phases of POM, probably with different

crystalline dimensions (Figure 3 c)), while the endothermic peak at 201 °C is probably due to the onset of POM decomposition, as identified from TGA (Figure 2 c)) [74]. The evaluation of X_c from the first heating scan is uncertain, since there is overlapping of the melting peak and the decomposition phenomena. It may be possible such an evaluation can be made using a deconvolution method to obtain three exothermic curves corresponding to each peak, in this way X_c is 48% only considering the two peaks at lower temperature. The second heating scan shows only a very small melting peak at 166 °C with a shoulder at 160°C, reflecting a very small degree of crystallinity, ~5%. Fractionated crystallisation in the cooling scan of the cured sample, shown in Figure 3 d), is still present, but the peaks are much less intense and that at 150 °C is almost suppressed. Similar behaviour was shown for the vulcanised samples (Table 3). The addition of the ionomer results in a decrease in X_c of the cross-linked samples compared to the uncross-linked sample, and the same trend, i.e. a decrease in X_c between the first and second heating cycles was also observed.

Table 3. Thermal parameters determined from DSC measurements for vulcanised EPDM:POM and EPDM:POM: Zn^{2+} Ionomer blends

Parameter	EPDM:POM	EPDM:POM -5	EPDM:POM -10	EPDM:POM -20
T_i	-	56	55	55
$T_{m,ion,1H}$	-	81	84	84
$T_{m,ion,2H}$	-	73	76	79
$T_{m,\ POM\ 1H}$	164-173	172	172	172
$T_{m\ POM,2H}$	167	168	168	169
$T_c$ion	-	44	45	46
$T_{c1,2,3}$ POM	93-124	-	-	97
$\Delta H_{m,1H}$ [J/g]	31.5	12.7	16.9	12.5
$X_{c,1H}$ [%]	48	20	28	23

$\Delta H_{m,2H}$ [J/g]	3.3	0.5	0.2	0.8
X_c,2H [%]	5	≈1	≈0	≈1

The X-Ray diffraction patterns of the cross-linked and uncross-linked blends are shown in Figure 4. All patterns show the presence of a broad curve with a peak maximum at 18.5°, mostly associated with the amorphous phases of the EPDM matrix, [49,75] and POM. The four peaks at 22.9°, 34.6°, 48.4° and 54.1° are characteristic of the hexagonal crystalline structure of POM and correspond to the {100}, {105}, {115} and {205} lattice planes, respectively [21] . It can be concluded that the blending process does not induce a variation of the POM crystalline phase. A comparison between the diffraction patterns of the uncross-linked and cross-linked samples shows the latter have sharper peaks, associated with the POM phase. In particular, the main (100) peak is more intense for the cured samples, hence it can be assumed that the curing process (i.e. application of temperature and pressure) results in an increase in the degree of crystallinity of the POM phase. This is agreement with the DSC analysis (see Figure 2 a)), which also confirmed increased crystallinity for vulcanised samples compared to uncured ones (Tables 2 and 3). On the other hand, sharper and narrower (100) peak was observed in the case of 8020 cured sample with respect to 8020-20 cured one, suggesting that ionomer induces a lower degree of crystallinity of POM phase characterized also by smaller crystallites [76]. The interaction between the ionic units of the ionomer and polar groups of POM restricts chain mobility, retards crystallization and decreases crystallinity [77,78]. Moreover, when the ionomer is added the (100) peak is shifted to lower theta angles confirming again some interaction between the blend components.

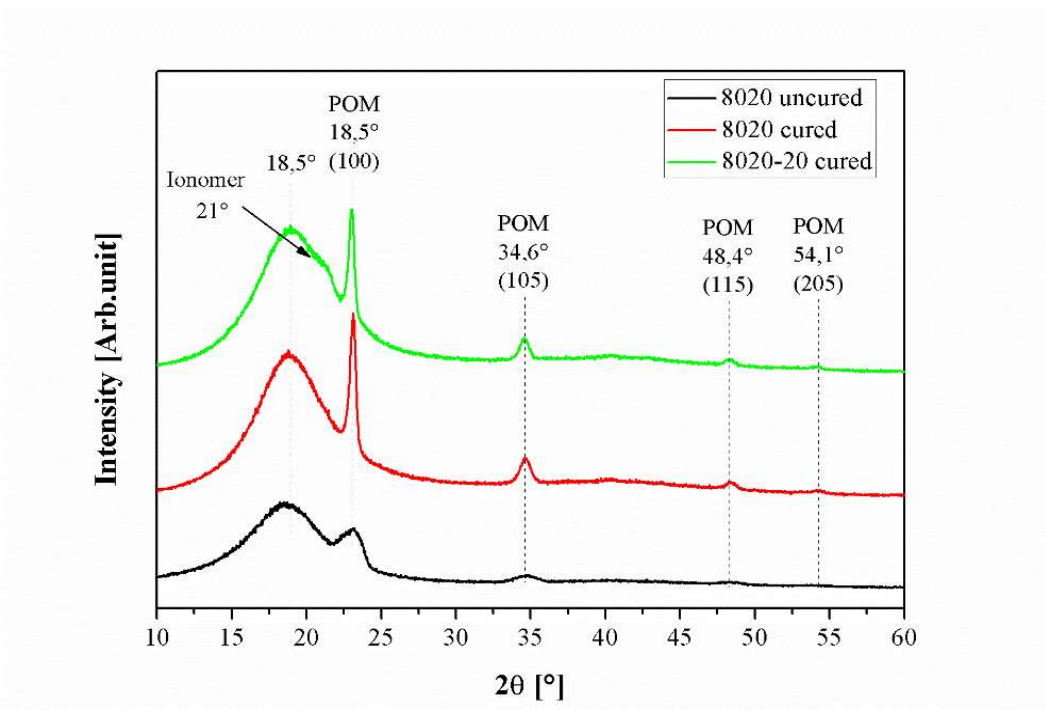

315

316 **Figure 4.** XRD curves for cured and uncured blends.

317

318 FTIR spectroscopy performed on the EPDM, POM, ionomer and the binary EPDM/POM and

319 ternary EPDM/POM/ Zn^{2+} ionomer blends was used to investigate if there were chemical interactions

320 between components in both uncross-linked and cross-linked blends.

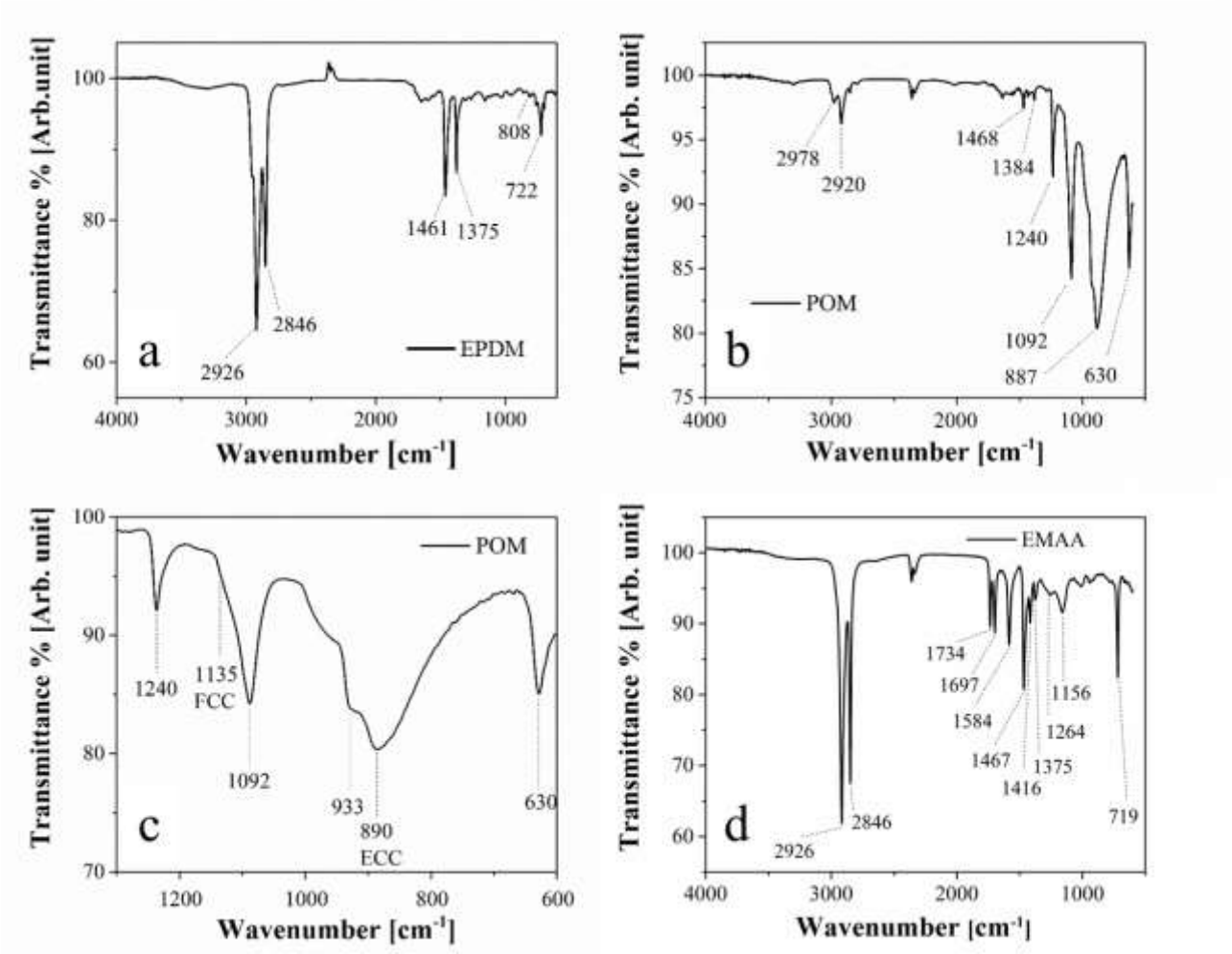

Figure 5. FTIR spectrum of EPDM (a), POM (b), expanded POM spectrum (c) and EMAA-Zn^{2+} (d)

The FTIR spectrum of the EPDM rubber shows peaks at 2926 cm^{-1} and 2846 cm^{-1} assigned to the saturated hydrocarbon backbone of aliphatic alkyl symmetric/asymmetric C−H stretching vibrations [79], Figure 5a). The peaks at 1461 cm^{-1} and 1375 cm^{-1} are due to $-CH_2-$ scissoring vibrations [80] and the symmetric C−H stretching vibration of $-CH_3$ from the propylene unit, respectively [81]. The peak at 808 cm^{-1} is characteristic of the olefinic alkene double bond (C=C) of the ENB [82] and, the peak at 722 cm^{-1} is assigned to $-(CH_2)_n-$, where $n \geq 5$, methylene rocking vibration due to presence of sequences of ethylene in the EPDM rubber backbone. The FTIR spectrum of POM and the most relevant vibrational band assignments are shown in Figure 5 b). The peaks at 2978 cm^{-1} and 2920 cm^{-1} are related to CH_2 symmetrical and asymmetrical stretching, and the peaks at 1468

333 cm^{-1} and 1384 cm^{-1} are due to CH_2 bending and wagging vibrations [83]. Peaks at 1240 cm^{-1}, 1092
334 cm^{-1} and 887 cm^{-1} are assigned to CH_2 rocking and C−O−C skeletal bending, asymmetric and
335 symmetric stretching, respectively. The bending of the O−C−O skeletal, along with CH_2 rocking is
336 observed at 630 cm^{-1} [84]. A summary of vibrational modes for the three investigated polymers is
337 reported in Table 4.

338 **Table 4**. Vibrational modes for EPDM, POM and EMAA-Zn^{2+}

Vibrational mode	**EPDM**	**POM**	**EMAA-Zn^{2+}**
CH_2 sym. stretch.	2926 cm^{-1}	2978 cm^{-1}	2926 cm^{-1}
CH_2 asym. stretch.	2846 cm^{-1}	2920 cm^{-1}	2846 cm^{-1}
C=O sym. stretch.	-	-	1734 cm^{-1}
C=O asym. stretch.	-	-	1697 cm^{-1}
C-O asym. stretch.	-	-	1584 cm^{-1}
CH_2 scissoring	1461 cm^{-1}	1468 cm^{-1}	1467; 1416 cm^{-1}
CH_2 wagging	-	1384 cm^{-1}	-
CH_3 sym. stretch.	1375 cm^{-1} (propylene unit)	-	1375 cm^{-1}
C-O-C bending	-	1240 cm^{-1}	1240 cm^{-1}
C-C-C streching	-	-	1156 cm^{-1}
C-O-C asym. stretch	-	1092 cm^{-1}	-
C=C sym. stretch	808 cm^{-1}	-	-
CH_2 rocking	722 cm^{-1}	1240; 630 cm^{-1}	719 cm^{-1}
C-O-C sym. stretch	-	887 cm^{-1}	-
O-C-O bending	-	630 cm^{-1}	-

339

POM, as stated above, can have two different morphologies, the folded-chain crystal (FCC) and extended-chain crystal (ECC), which can be readily distinguished from FTIR spectra in the region 1200 cm^{-1} -700 cm^{-1} [85]. It is known that four bands at 1240 cm^{-1}, 1092 cm^{-1}, 933 cm^{-1} and 630 cm^{-1} are independent of POM morphology, while the bands around 1135 cm^{-1} and 900 cm^{-1} are characteristic of FCC and ECC morphology, respectively [69]. Expansion of the FTIR spectrum of in the region 1300 cm^{-1}-600 cm^{-1} is shown in Figure 5 c). The POM does not contain any FCC morphology as the peak at 1135 $cm^{-1}$is absent, but is most probably formed of ECC morphology due to the presence of a highly intense peak at 890 cm^{-1} [86,87], in agreement with conclusions made from the DSC data.

The FTIR spectra of the binary blend of EPDM:POM (80:20), both uncross-linked and cross-linked are shown in Figure 6 a). The spectrum of the uncured sample seems to be a superposition of the POM and EPDM spectra, showing peaks characteristic of both polymers, thus indicating no interaction between the two materials. The only major change is that the peak at 890 cm^{-1}, derived from the ECC morphology of POM, is shifted to 904 cm^{-1}, is lower in intensity and, at the wavenumber usually reported in literature for the ECC peak [84,88]. These results suggest that the POM phase in the blend has now a mixed morphology of FCC and ECC since the most intense peaks are those assigned to both morphologies (935 cm^{-1}, 1092 cm^{-1} and 1240 cm^{-1}) [69,88]. However, significant differences can be seen in the spectrum of the vulcanised sample. In particular, the bands at 1240 cm^{-1} and 1092 cm^{-1} are much more intense than that for the uncross-linked samples and a new peak evolves at 1118 cm^{-1} and a shoulder process at 975 cm^{-1} (Figure 6 b)). These bands are ascribed to POM chain vibrations and their high intensities to a change in the degree of crystallinity, as reported previously [89] and, confirmed by the XRD and DSC studies (see Tables 2 and 3) which showed that the crystallinity of the cross-linked sample is twice (48%) that of the uncross-linked sample (23%). Moreover, the peak at 1155 cm^{-1} is very intense in the cured sample while the peak at 904 cm^{-1} is now absent. This can be explained by a rearrangement of the FCC and ECC morphologies of the POM phase during the thermal treatment associated with curing.

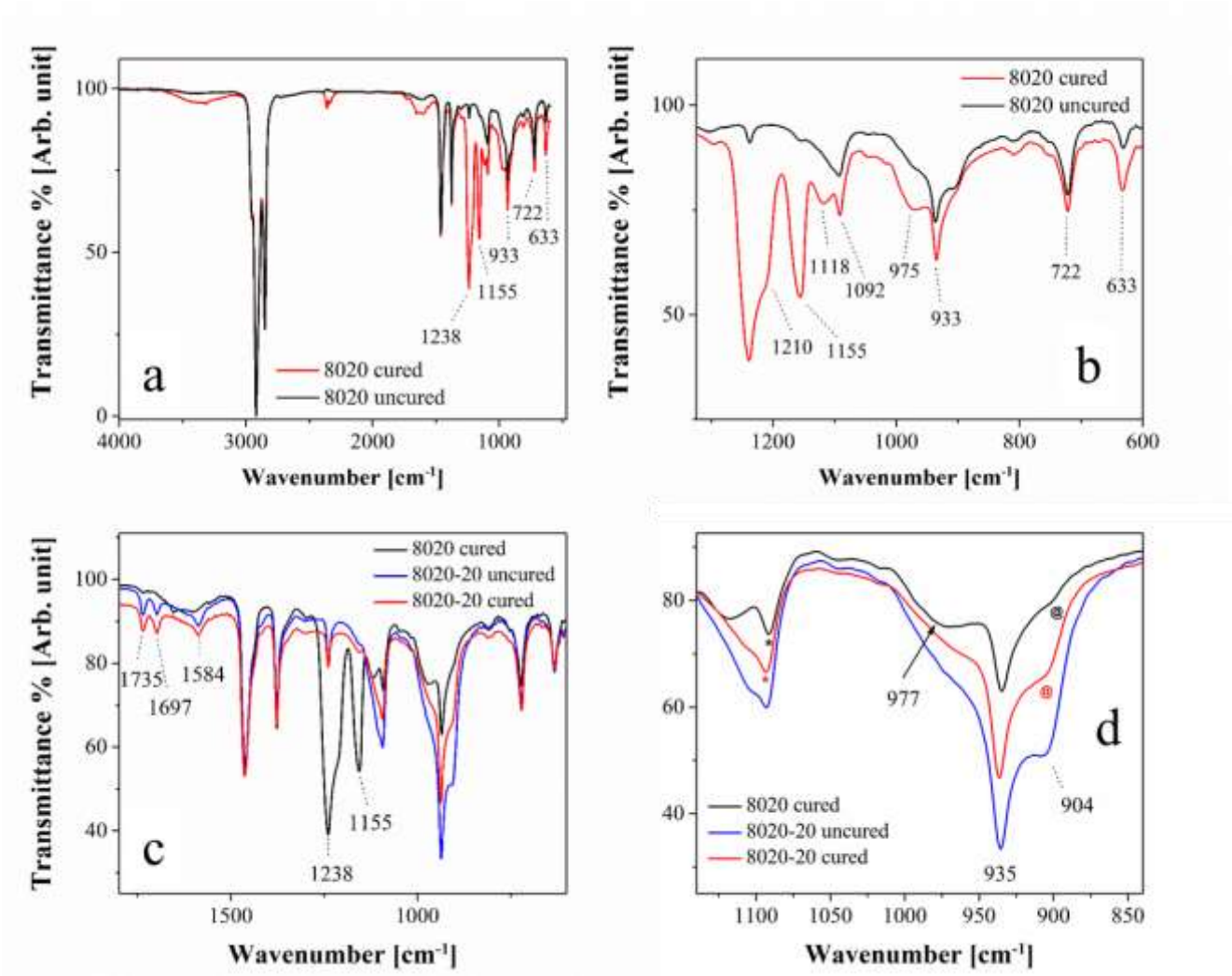

Figure 6. FTIR spectra comparing a) EPDM:POM cross-linked and uncross-linked blends, b) as in a) expanded in the range 1200-600 cm^{-1} and, c) EPDM:POM:Zn^{2+} Ionomer cross-linked and uncross-linked blends and d) as in c) expanded in the range 1200-600 cm^{-1}.

Comparison of the FTIR spectra in the wavenumber range 1800-600 cm^{-1}, of the crosslinked EPDM:POM blend with the uncross-linked and cross-linked EPDM:POM:Zn^{2+} Ionomer blends are shown in Figure 6 c). It can be seen that there are peaks present due to the presence of the ionomer. These ionomer related peaks (Figure 5 d)), such as those at 1734 cm^{-1} and 1697 cm^{-1} are ascribed to ester carbonyl group and carboxylic acid group, and the peak at 1584 cm^{-1} is related to the asymmetric stretching vibration of the C−O bond in tetra-coordinated zinc carboxylates [90–92]. FTIR measurements confirmed that there is an interaction between the ionomer and the other components of the blend. In particular a slight shift to higher wavenumber for C-O vibrations of POM (indicated by the symbols

* and @ in Figure 6 d)) and of Zn^{2+} ionomer due to the interaction between the pedant ions of EMAA-Zn^{2+} and the dipoles of POM was detected. Moreover, the inclusion of the ionomer results in lower POM crystallinity and has a major influence on the folded-chain crystal (FCC) and extended-chain crystal (ECC) morphology of POM. Indeed, from Figure 6 d) the evolution of a peak at 904 cm^{-1} is clear, directly related to ECC morphology, both in the uncured and cured 80:20-20 samples. Hence the presence of the ionomer promotes ECC morphology of the POM phase.

The dynamic mechanical properties of neat EPDM, POM and EMAA-Zn^{2+} and their blends are reported in Figure 7. EPDM (Figure 7 a)) has a glass transition temperature (T_g) at −49.2 °C, coincidently similar to the T_g value (−52 °C) determined by DSC. The storage modulus (E′) at low temperature (−100 °C) is 1.52 GPa, and at RT (20 °C) is 6.25 MPa. The loss tangent (tanδ), which is the ratio between the loss modulus (E″) and the storage modulus (E′) and a measure of the "damping" properties, reaches 1.2, showing the high dissipating properties of EPDM rubber. POM (Figure 7 b)) has a T_g at −66 °C and, a E′ value at low temperature (−100 °C) of 3.93 GPa but at RT (20 °C) 1.75 GPa.

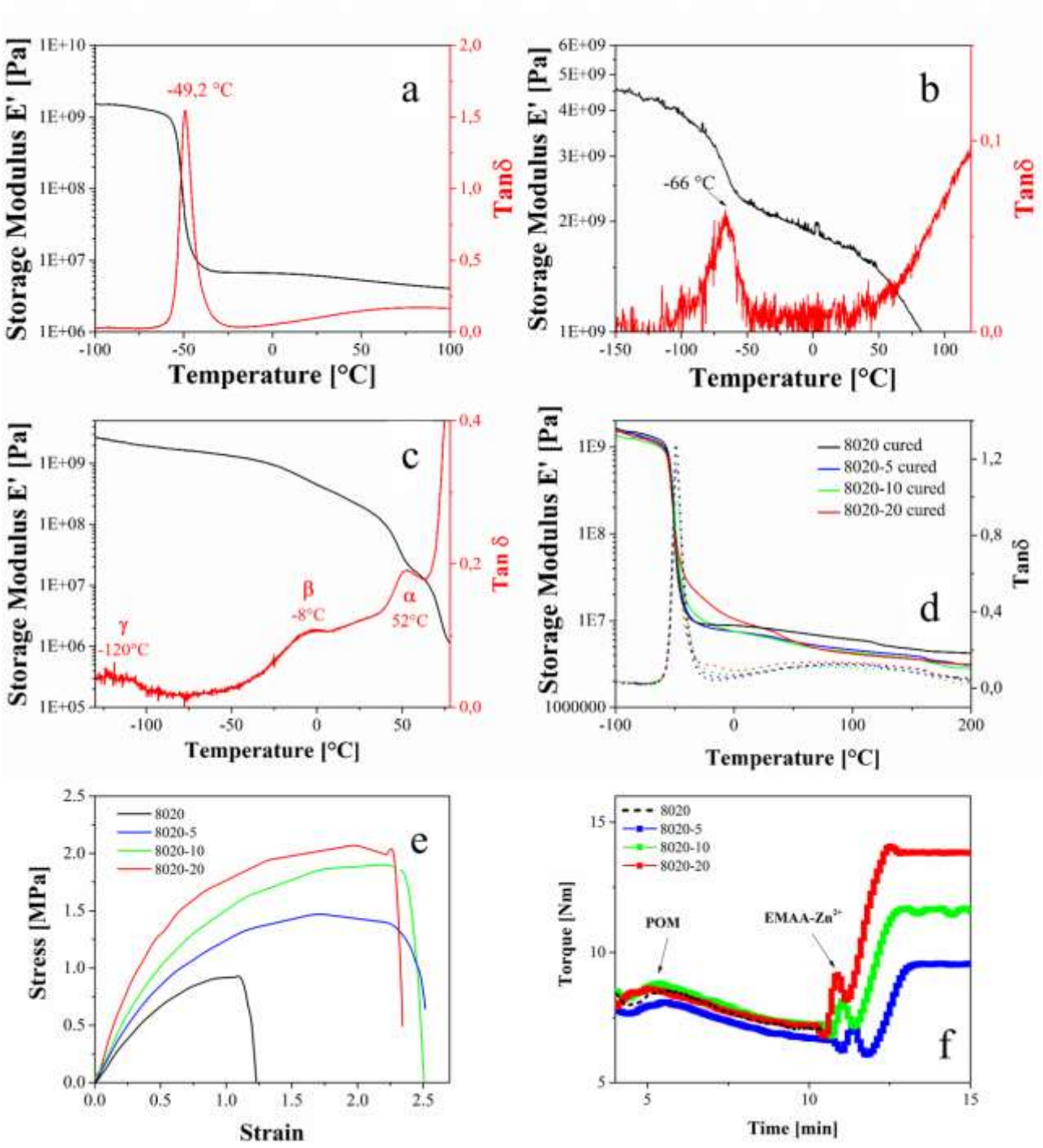

Figure 7. Variation in E′ and tan δ as a function of temperature for a) cured EPDM, b) POM, c) EMAA-Zn^{2+} and d) all cured blends. e) Representative stress-strain curves for cured blends. f) rheological behaviour comparison

Moreover, upon approaching the T_m of POM a further decrease in E′ can be seen at about 100 °C, which is often called the αc transition ($T_{\alpha c}$) and is attributed to the reorientation of the chains in the crystalline phase [93]. In contrast, the EMAA-Zn^{2+} (Figure 7 c)) displays different behaviour. At −120

°C there is a broad γ relaxation peak ascribed to the crankshaft motion of short hydrocarbon segments in the amorphous phase. A second peak at around −8 °C is assigned to β relaxation occurring in the amorphous branched polyethylene phase where most of the ionic species is not present [42]. Lastly, the α relaxation occurs at 52 °C and is caused by the mobility of the ionic phase (order-disorder of ionic cluster transition), it can be considered as the glass transition temperature (T_i) of the ionic clusters, and it is function of neutralisation and ion content [94].

All blends exhibit a single glass T_g around −49 °C (Figure 7 d), Table 5) from the EPDM matrix, as it is the main component of all the blends. This result could be misinterpreted as an indication of compatibilization, as the presence of a single T_g in blends is a criterion commonly used to judge blend miscibility. However, in this instance this would be misleading as change in T_g can only be considered a reliable indicator of miscibility when the difference between the $T_{g's}$ of the single constituents in the blend ≥20 °C [1]. This is not the case here as EPDM and POM have $T_{g's}$ of -49 °C and −66 °C, respectively. Moreover, it has been reported that, even for immiscible blends, rarely are two $T_{g's}$ detected for blends when the dispersed phase is < 20 wt% of the blend composition [2], as in this case. The addition of the ionomer to the EPDM:POM blend results in a decrease in the intensity of the loss tangent peak and, hence, of damping capacity.

Table 5. Storage modulus (E′) values at -85 °C and 20 °C and, glass transition temperatures (T_g) and loss tangent (tan δ) maxima of cured samples.

Sample	E'_{-85} [GPa]	E'_{20} [MPa]	T_g [°C]	tanδ max
EPDM:POM	1.48	8.35	−49	1.28
EPDM:POM-5	1.30	6.85	−49.1	1.15
EPDM:POM-10	1.25	8.52	−49.1	0.96
EPDM:POM-20	1.33	11.49	−49.2	0.76

The tensile mechanical properties of EPDM, EPDM:POM and EPDM:POM:Zn^{2+} Ionomer materials were measured, and the results summarised in Table 6. The cured blends display

thermoplastic-like behaviour (Figure 7 e)), which is very common for thermoplastic-elastomer blends [20]. The elastic modulus for the EPDM:POM sample increased relative to neat EPDM, but σ_{max} decreased, as expected, indicating poor stress transfer to the POM dispersed phase. It can be supposed that the dispersed phase acts as stiffener for the EPDM matrix obstructing EPDM chain sliding, but it does not improve tensile strength due to a weak interface, again confirming the immiscibility of the EPDM/POM system [12], as seen from the FT-IR measurements.

Table 6. Tensile mechanical properties and Hardness values for cured samples.

Sample	E [kPa]	σ_{max} [kPa]	ε_{max} [%]	Absorbed energy [kJ/m^3]	Hardness [Shore A]
EPDM	2.60±0.58	1140± 113	101.5±19.1	753±24	50.2±1.1
EPDM:POM	4.57±0.73	780 ± 56	107.7±22.5	776±58	56.8±1.3
EPDM:POM-5	5.36±1.30	1290 ± 140	190.0±41.9	2870±61	59.8±1.2
EPDM:POM-10	5.34±1.09	1480 ± 130	196.3±39.7	3580±49	62.9±0.8
EPDM:POM-20	7.05±1.69	1870 ± 143	211.8±8.2	3800±63	70.1±1.3

The addition of the ionomer results in an overall increase in all mechanical properties, including elastic modulus (E), tensile strength (σ) and elongation at break (ε). In the best case (EPDM:POM-20) the elastic modulus increases up to 54%, tensile strength up to 139% and elongation at break up to 97% suggesting a strong interfacial adhesion between POM and the EPDM matrix. Shore A hardness also increases, almost linearly with ionomer amount, supporting the concept that the presence of the ionomer promotes compatibilization. Moreover, the absorbed energy given by integrating the stress strain curves displays an increase with the presence of ionomer. Absorbed energy is strictly related to toughness and the increase suggests that EPDM and POM are compatibilized by the ionomer. These results are also in agreement with the evolution of torque acquired during mixing, see Figure 7 f). The two peaks observed in each torque curve are ascribed to the loading and melting of POM and Zn^{2+} ionomer. In agreement with the published literature [9,95], an increase in torque with increasing EMAA-Zn^{2+} content is observed. Such an effect can be ascribed to an optimized interfacial tension and a stabilization of the dispersed POM droplets, resulting in a finer POM dispersed phase [96].

446 This hypothesis was further confirmed by imaging the blends by SEM, Figure 8. For the
447 EPDM:POM blend, the POM dispersed phase is irregular shaped with a broad size distribution (figure
448 8 a)), although uniformly dispersed throughout the rubber matrix. In the samples etched with acetic
449 acid, POM crystalline regions (highlighted by the red arrows in figure 8b)) can be seen within the
450 EPDM matrix, along with voids where etching has removed the POM amorphous phase. The cryo-
451 fractured surface of the cured EPDM:POM sample after etching with sodium hydroxide for 24 hours
452 offers more convincing evidence, as etching is stronger and results in the complete removal of the
453 POM dispersed phase leaving only empty voids having dimensions of 10.78 ± 1.36 μm, from
454 exhaustive image analysis of many images.

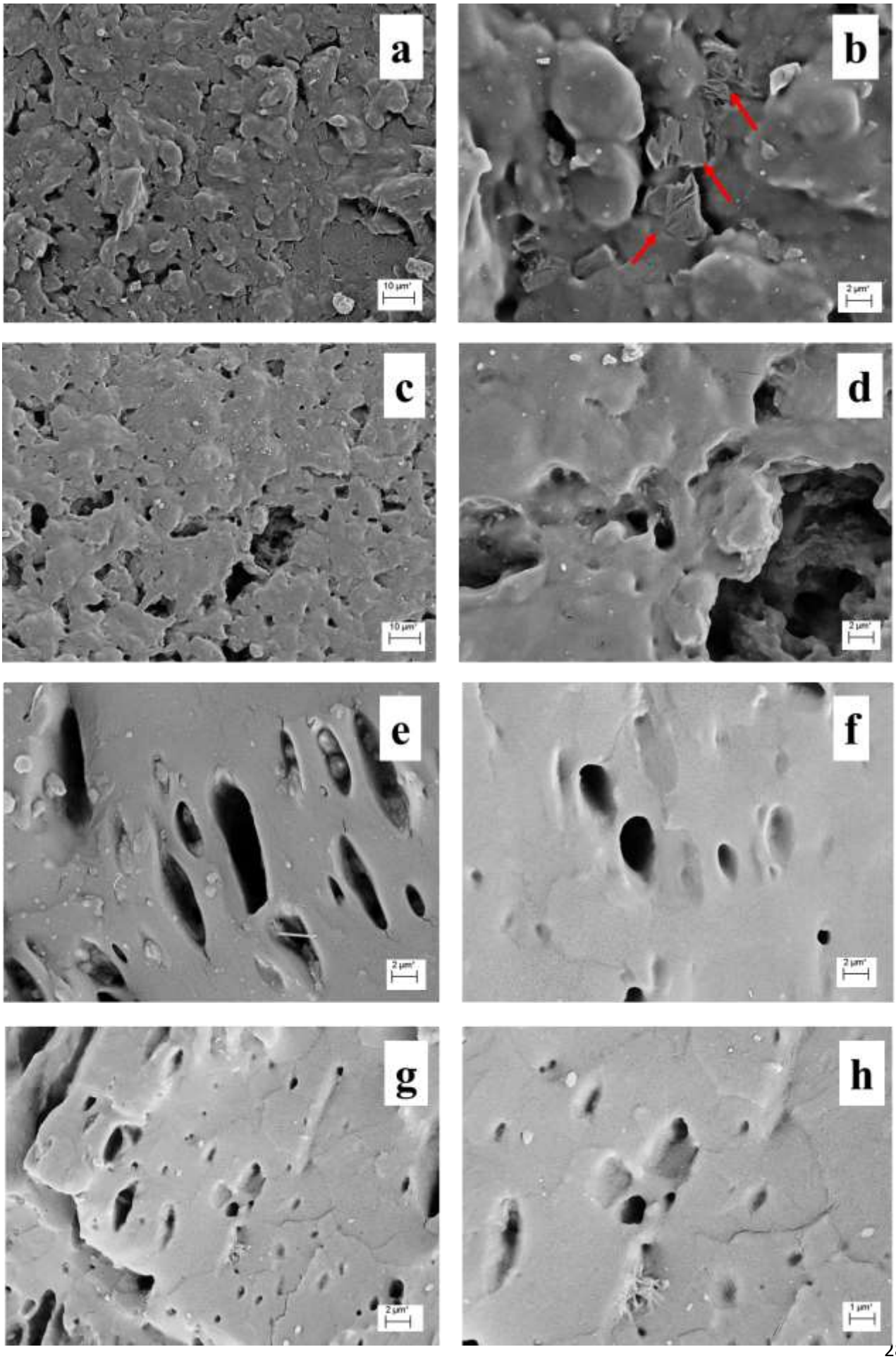

455

Figure 8. SEM images at a) low and b) high magnification of the acetic acid etched EPDM:POM blend, (c) low and (d) high magnification of the NaOH etched EPDM:POM blend and, the EPDM:POM:Zn^{2+} Ionomer blend with e) 5 wt%, f) 10 wt%, g) and h) 20 wt% ionomer content.

The SEM images of cryo-fractured cured EPDM:POM:Ionomer blends etched with sodium hydroxide for 24 hours, shows the addition of the ionomer changed the morphology of the blend. The POM phase is dispersed uniformly and in smaller domains having dimensions less than that observed for the EPDM:POM blend. Specifically, with increasing ionomer content from 5 wt% to 10 wt% and then 20 wt%, the dimensions of the POM phase decreased from 10.78 ± 1.36 μm (figure 8 c) d)) to 6.21 ± 1.89 μm (figure 8 e)), 2.93 ± 1.01 μm (figure 8 f) and 1.29 ± 0.65 μm (figure 8 g) h), respectively.

4. Conclusions

An immiscible blend of EPDM and POM was partly compatibilized using a commercial Zn^{2+} ionomer, poly(ethylene-co-methacrylic acid)-Zn^{2+}. Blends with a fixed 80:20 EPDM:POM ratio and different ionomer content, up to 20 wt%, were obtained through melt mixing followed by vulcanization. DSC analysis of the binary EPDM:POM blends exhibited fractionated crystallisation of the POM dispersed phase, which was more evident for uncured samples. The addition of the Zn^{2+} ionomer shifted crystallisation towards lower temperatures due to the decrease in the size of the POM domains and also resulted in a decrease in POM crystalline content. Moreover, the blending process diminished the thermal stability of all blends as seen from TGA. FTIR analysis showed the POM dispersed phase changed from a predominantly ECC morphology to a mixed FCC and ECC morphology. On addition of ionomer to the EPDM:POM blend, the evolution of new peaks associated with the ionomer were observed in the FTIR spectra. The crystal phases of all components were not affected by the blending process as confirmed by XRD. DMTA revealed the cured samples displayed only one T_g ascribed to the EPDM rubber matrix. Nevertheless, the closeness of the $T_{g's}$ of the blend

components when the POM content is <20 wt%, cannot be taken as evidence of compatibilization. The immiscible EPDM:POM binary blend had poor mechanical properties, as expected, however addition of the ionomer reduced interfacial tension and compatibilized EPDM and POM. The resultant blends had significantly improved elastic modulus, tensile strength and toughness and, elongation at break. The enhanced interfacial interactions between the blend components on inclusion of the ionomer was manifest by a decrease in the size and surface area of the POM phase (droplets), confirmed from SEM imaging of etched samples.

Acknowledgments

The authors thank Mr. Riccardo Campana for technical assistance. V.C. thanks the IINM, WMG, University of Warwick, UK for hosting her research visit.

References

1. Robeson, L. M. *Polymer Blends*; Hanser Gardner Publications, Inc, **2007**.
2. Utracki, L. A.; Wilkie, C. A. *Polymer blends handbook*; **2014**.
3. Thomas, S.; Shanks, R.; Chandrasekharakurup, S. *Nanostructured Polymer Blends*; **2014**.
4. Jolfaei, A. F.; Gavgani, J. N.; Jalali, A.; Goharpey, F. *Polym. Bull.* **2015**, *72*, 1127.
5. Michler, G. H.; Michler, G. H. *Polymer Blends*; **2016**.
6. Paul, D. R.; Barlow, J. W. **1979**, 315.
7. Abitha, V. K.; Rane, A. V. *Res. Rev. Polym.* **2014**, *5*, 102.
8. Razavi Nouri, M.; Mehrabzadeh, M. *Iran. Polym. J. (English Ed.* **1996**, *5*, 237.
9. Moghaddam, M. P.; Abdi, H.; Javidi, M. H. *Iran. Polym. J.* **2008**, *17*, 669.
10. Nicolini, A.; De Campos Rocha, T. L. Á.; Jacobi, M. A. M. *J. Elastomers Plast.* **2009**, *41*, 433.
11. Stelescu, D. M.; Airinei, A.; Homocianu, M.; Fifere, N.; Timpu, D.; Aflori, M. *Polym. Test.* **2013**, *32*, 187.
12. Chiang, W. -Y; Huang, C. -Y *J. Appl. Polym. Sci.* **1993**, *47*, 105.
13. Ghosh, P.; Chattopadhyay, B.; Sen, A. K. *Polymer (Guildf).* **1994**, *35*, 3958.

14. Uthaman, R. N.; Pandurangan, A.; Majeed, S. S. M. A. *J. Polym. Res.* **2007**, *14*, 441.

15. BF, A. *MOJ Polym. Sci.* **2017**, *1*, 5.

16. Sadiku, R.; Ibrahim, D.; Agboola, O.; Owonubi, S. J.; Fasiku, V. O.; Kupolati, W. K.; Jamiru, T.; Eze, A. A.; Adekomaya, O. S.; Varaprasad, K.; Agwuncha, S. C.; Reddy, A. B.; Manjula, B.; Oboirien, B.; Nkuna, C.; Dludlu, M.; Adeyeye, A.; Osholana, T. S.; Phiri, G.; Durowoju, O.; Olubambi, P. A.; Biotidara, F.; Ramakokovhu, M.; Shongwe, B.; Ojijo, V. In *Polyolefin Fibres: Structure, Properties and Industrial Applications: Second Edition*; **2017**; pp 81.

17. Sharks, R.; Kong, I. In *Thermoplastic Elastomers*; El-Sonbati, A., Ed.; **2016**; pp 653.

18. Spontak, R. J.; Patel, N. P. *Curr. Opin. Colloid Interface Sci.* **2000**, *5*, 333.

19. Drobny, J. G. *Handbook of Thermoplastic Elastomers*; **2007**.

20. Sharma, B. K.; Chowdhury, S. R.; Mahanwar, P. A.; Sarma, K. S. S. *Adv. Mater. Phys. Chem.* **2015**, *05*, 383.

21. L, S. L.; P.M, V.; Chandran, S. *Polyoxymethylene Handbook*; Wiley, **2014**.

22. Uthaman, N.; Majeed, A.; Pandurangan *E-Polymers* **2006**, 1.

23. Banerjee, S. S.; Bhowmick, A. K. *Rubber Chem. Technol.* **2017**, *90*, 1.

24. Kumar, G.; Neelakantan, N. R.; Subramanian, N. *J. Appl. Polym. Sci.* **1994**, *52*, 483.

25. Oh, J. S.; Isayev, A. I. *J. Appl. Polym. Sci.* **2004**, *93*, 1166.

26. Uthaman, R. N.; Pandurangan, A.; Majeed, S. S. M. A. *Polym. Eng. Sci.* **2007**, 934.

27. Bouchart, V.; Bhatnagar, N.; Brieu, M.; Ghosh, A. K.; Kondo, D. *Comptes Rendus - Mec.* **2008**, *336*, 714.

28. Huang, J. M.; Cheng, H. J.; Wu, J. S.; Chang, F. C. *J. Appl. Polym. Sci.* **2003**, *89*, 1471.

29. Naskar, K.; Noordermeer, J. W. M. *J. Appl. Polym. Sci.* **2006**, *100*, 3877.

30. Xie, H. Q.; Feng, D. S.; Guo, J. S. *J. Appl. Polym. Sci.* **1997**, *64*, 329.

31. Wouters, M. E. L. *Ionomeric Thermoplastic Elastomers based on Ethylene-Propylene Copolymers*; **2000**.

32. R. W. Rees and D. J. Vaughan **1965**, 296.

33. Eisenberg, A.; Rinaudo, M. *Polym. Bull.* **1990**, *24*, 671.

34. Eisenberg; Kim In *Inroduction to Ionomers*; Wiley, **1998**; pp 1.

35. *Structure and Properties of lonomers*; Pineri, M.; Eisenberg, A., Eds.; D. Reidel Publishing Company, **1986**.

36. Zhang, L.; Brostowitz, N. R.; Cavicchi, K. A.; Weiss, R. A. *Macromol. React. Eng.* **2014**, *8*, 81.

37. Tant, M. R.; Mauritz, K. A.; Wilkes, G. L. *Ionomers*; PROFESSIONAL, L. A. &, Ed.

38. Utracki, L. A. *Multiphase Polymers: Blends and Ionomers*; **1989**; Vol. 395.

39. Hara, M.; Eisenberg, A. *Macromolecules* **1987**, *20*, 2160.

40. Horrion, J.; Cartasegna, S.; Agarwal, P. K. *Polym. Eng. Sci.* **1996**, *36*, 2061.

41. Wang, X.; Cui, X. *Eur. Polym. J.* **2005**, *41*, 871.

42. MacKnight, W. J.; Earnest, T. R. *J. Polym. Sci. Macromol. Rev.* **1981**, *16*, 41.

43. Penco, M.; Rhaman, A.; Spagnoli, G.; Janszen, G.; Di Landro, L. *Mater. Lett.* **2011**, *65*, 2107.

44. Hohlbein, N.; Shaaban, A.; Bras, A. R.; Pyckhout-Hintzen, W.; Schmidt, A. M. *Phys. Chem. Chem. Phys.* **2015**, *17*, 21005.

45. Lüftl, S.; Visakh, P. M. *Polyoxymethylene Handb. Struct. Prop. Appl. their Nanocomposites* **2014**, 1.

46. Sichina, W. J. Characterization of EPDM Elastomers Using DSC. *Perkin Elmer instruments* **2000**, 1–3.

47. Determination of crystallinity, MettlerToledo T A Application Handbook Elastomers Volume 1 **2002**, *1*, 1–3.

48. Ver Strate, G.; Wilchinsky, Z. W. *J. Polym. Sci. Part A-2 Polym. Phys.* **1971**, *9*, 127.

49. Gilbert, M.; Briggs, J. E.; Omana, W. *Br. Polym. J.* **1979**, *11*, 81.

50. De Santis, F.; Gnerre, C.; Nobile, M. R.; Lamberti, G. *Polym. Test.* **2017**, *57*, 203.

51. Jaffe, M.; Wunderlich, B. *Kolloid-Zeitschrift und Zeitschrift für Polym.* **1967**, *216–217*, 203.

52. Coopert, S. L. *J. Macromol. Sci. Part B* **1974**, *9*, 19.

53. Loo, Y. L.; Wakabayashi, K.; Huang, Y. E.; Register, R. A.; Hsiao, B. S. *Polymer (Guildf).* **2005**, *46*, 5118.

54. Dolog, R.; Weiss, R. A. *Macromolecules* **2013**, *46*, 7845.

55. Tadano, K.; Hirasawa, E.; Yamamoto, H.; Yano, S. *Macromolecules* **1989**, *22*, 226.

56. Lu, L.; Li, G. *ACS Appl. Mater. Interfaces* **2016**, *8*, 14812.

57. Ray, A. K. *J. Therm. Anal.* **1996**, *46*, 1527.

58. Kongkhlang, T.; Reddy, K. R.; Kitano, T.; Nishu, T.; Tashiro, K. *Polym. J.* **2011**, *43*, 66.

59. Kusy, R. P.; Whitley, J. Q. *Am. J. Orthod. Dentofac. Orthop.* **2005**, *127*, 420.

60. Archodoulaki, V. M.; Lüftl, S.; Koch, T.; Seidler, S. *Polym. Degrad. Stab.* **2007**, *92*, 2181.

61. Santana, O. O.; Müller, A. J. *Polym. Bull.* **1994**, *32*, 471.

62. Everaert, V.; Groeninckx, G.; Aerts, L. *Polymer (Guildf).* **2000**, *41*, 1409.

63. Koutsky, J. A.; Walton, A. G.; Baer, E. *J. Appl. Phys.* **1967**, *38*, 1832.

64. Langhe, D. In *Crystallization in Multiphase Polymer Systems*; **2018**; pp 239.

65. Langhe, D. In *Multiphase Polymer Systems*; **2018**; pp 239.

66. Groeninckx, G.; Harrats, C.; Vanneste, M.; Everaert, V. In *Polymer Blends Handbook*; **2014**; pp 1.

67. Klemmer, N.; Jungnickel, B. J. *Colloid Polym. Sci.* **1984**, *262*, 381.

68. Barczewski, M.; Matykiewicz, D.; Andrzejewski, J. *Macromol. Res.* **2015**, *23*, 850.

69. Chen, Z.; Zhou, T.; Hui, J.; Li, L.; Li, Y.; Zhang, A.; Yuan, T. *Vib. Spectrosc.* **2012**, *62*, 299.

70. Tang, T.; Huang, B. *J. Appl. Polym. Sci.* **1994**, *53*, 355.

71. Everaert, V.; Groeninckx, G.; Koch, M. H. J.; Reynaers, H. *Polymer (Guildf).* **2003**, *44*, 3491.

72. Calderón, B. A.; Sobkowicz, M. J. *J. Appl. Polym. Sci.* **2018**, *135*, 1.

73. Luo, H.; Huang, Y.; Wang, D. *Eur. Polym. J.* **2013**, *49*, 1424.

74. Lüftl, S.; Archodoulaki, V. M.; Seidler, S. *Kunststoffe Plast Eur.* **2001**, *91*, 40.

75. Valentini, L.; Bittolo Bon, S.; Lopez-Manchado, M. A.; Verdejo, R.; Pappalardo, L.; Bolognini, A.; Alvino, A.; Borsini, S.; Berardo, A.; Pugno, N. M. *Compos. Sci. Technol.* **2016**, *128*, 123.

76. Ardanuy, M.; Velasco, J. I.; Maspoch, M. L.; Haurie, L.; Fernandez, A. I. *J. Appl. Polym. Sci.* **2009**, *113*, 950.

77. Hu, Y. S.; Prattipati, V.; Mehta, S.; Schiraldi, D. A.; Hiltner, A.; Baer, E. *Polymer (Guildf).* **2005**, *46*, 2685.

78. Ju, L.; Mondschein, R. J.; Vandenbrande, J. A.; Arrington, C. B.; Long, T. E.; Moore, R. B. *Polymer (Guildf).* **2020**, *205*, 122891.

79. Bragaglia, M.; Lamastra, F. R.; Cherubini, V.; Nanni, F. *Express Polym. Lett.* **2020**, *14*.

80. Bragaglia, M.; Cacciotti, I.; Cherubini, V.; Nanni, F. *Wear* **2019**, *434–435*.

81. Gunasekaran, S.; Natarajan, R. K.; Kala, A. *Spectrochim. Acta - Part A Mol. Biomol. Spectrosc.* **2007**, *68*, 323.

82. Vadivel, M.; Shobana, S.; Narayan, S. A.; Mitu, L.; Raja, J. D.; Sankarganesh, M. *Bulg. Chem. Commun.* **2017**, *49*, 26.

83. Loo, L. S.; Gleason, K. K. *Electrochem. Solid-State Lett.* **2001**, *4*, 81.

84. Li, Y.; Zhou, T.; Chen, Z.; Hui, J.; Li, L.; Zhang, A. *Polymer (Guildf).* **2011**, *52*, 2059.

85. Zamboni, V.; Zerbi, G. *J. Polym. Sci. Part C Polym. Symp.* **2007**, *7*, 153.

86. Chang, F. C.; Yang, M. Y.; Wu, J. S. *Polymer (Guildf).* **1991**, *32*, 1394.

87. Shimomura, M.; Iguchi, M. *Polymer (Guildf).* **1982**, *23*, 509.

88. Hama, H.; Tashiro, K. *Polymer (Guildf).* **2003**, *44*, 3107.

89. Hagemann, H.; Snyder, R. G.; Peacock, A. J.; Mandelkern, L. *Macromolecules* **1989**, *22*, 3600.

90. Coleman, M. M.; Lee, J. Y.; Painter, P. C. *Macromolecules* **1990**, *23*, 2339.

91. Kutsumizu, S.; Hara, H.; Tachino, H. *Macromolecules* **1999**, *32*, 6340.

92. Zeng, X.; Yamane, H.; Takahashi, M.; Masuda, T. *Zair. Soc. Mater. Sci. Japan* **1999**, *48*, 28.

93. Rault, J. *J. Macromol. Sci. - Rev. Macromol. Chem. Phys.* **1997**, *37*, 335.

94. Tachino, H.; Hara, H.; Hirasawa, E.; Kutsumizu, S.; Tadano, K.; Yano, S. *Macromolecules* **1993**, *26*, 752.

95. Xu, C.; Lin, B.; Liang, X.; Chen, Y. *Ind. Eng. Chem. Res.* **2016**, *55*, 4539.

96. Utracki, L. A. *Can. J. Chem. Eng.* **2002**, *80*, 1008.